Supplementary material for

Topographic asymmetry of the South Atlantic from global models of mantle flow and lithospheric stretching

Flament et al.

Earth and Planetary Science Letters

1. Kinematic models for deforming regions

The methodology for building deforming regions into global plate reconstructions builds on the continuously closing plates framework described by Gurnis et al. (2012). Plates are defined within the open-source software *GPlates* (Boyden et al., 2011) by building polygons from a series of lines defining plate boundaries. The lines can move independently, so that the geometry of plate polygons continually change as a function of reconstruction time. Within this original framework, plate velocities within each plate polygons were based on the stage rotation of that plate (*i.e.* plates were considered internally 'rigid', but with crust being accreted or destroyed at the plate boundaries).

The kinematic models used in this paper use an adaptation of the continuously closing plates methodology to allow deformation within certain regions. Similar to the original continuously closing plates concept, the boundaries of deforming regions are built within *GPlates* from a series of lines and points. These lines and points have their own motion history such that the deforming regions can change geometry over time. However, within deforming regions, the plate velocities are not calculated from a single stage pole - instead, they

are derived by interpolation of velocities from points on the boundaries of the deforming regions, as well as additional constraints within the deforming zones (lines, points or smaller 'rigid' polygons) whose motion is constrained by geological observation. Figs. 1 and 2 show the regions of deformation within our model - the methodology used to delineate the extent of these regions is also discussed in Section 2.4 of the main text.

For example, our models incorporate a representation of deformation within the Andes from 45 Ma to present day. The kinematic model, covering the area shown by the green hatching in Figs. 1 and 2, is based on the study of Arriagada et al. (2008), who derived 2D map restorations of the central Andes using a combination tectonic shortening estimates and paleomagnetic rotations. In our reconstructions, a series of points within individual motion histories are defined both along the Andean margin and within the region of Andean crustal shortening, providing a representation both of crustal shortening and the changing geometry of the Andean convergent margin.

A different approach is required for conjugate passive margins. For these regions, we use a method similar to that described by Srivastava and Verhoef (1992). To construct kinematic models of margin extension and breakup that remain topologically correct for all reconstruction times, we first define the extent of extended continental crust within each margin. We start with a set of continent-ocean boundaries (COBs) on the conjugate margins and a series of finite rotations that describes the relative motion between the plate-pair (for example, rotations between South America and Southern Africa) beginning from the onset of rifting. Given this information, we can create a set of vertices on the conjugate COB lines that map onto each other during

the reconstruction. Each vertex on each COB has an individual motion history. The motion history is derived from the combination of geometries and finite rotations, so that topological correctness is preserved at all times. For times when 'rigid' COBs would imply overlap between the conjugate margins, COB points move along small circle paths defined by the stage pole of the rigid plate pair. The magnitude of the motion is calculated to preserve the present-day ratio of the widths of the conjugate margins. Following this method, we can derive a kinematic model that describes progressive breakup and onset of seafloor spreading. For example, Figs. 3C and F (main text) show a stage in the South Atlantic where breakup has already occurred in the southern South Atlantic (so plate velocities here are consistent with the stage pole for South America), while extension continues in the Equatorial Atlantic and plate velocities within the deforming regions are derived by linear interpolation from the surrounding constraints.

Definition of deforming regions is more straightforward for regions within Africa and South America where rifting did not proceed to breakup. In both the models tested here the African continent comprises rigid blocks separated by regions of deformation that correspond to fairly well known rift basins which formed contemporaneously with South Atlantic opening (see Torsvik et al., 2009 and Heine et al., 2013 for further discussion). Cretaceous deformation within South America in both models is confined to the southern part of the continent. In the case of the Torsvik et al. (2009) model, the extent of the areas affected by extension and oblique transtension between the Colorado, Paraná and Amazonia blocks is not explicitly illustrated, and additional data to define the extent of these basins is lacking. We have

defined regions $\sim$ 150 km wide to accommodate this deformation.

2. Model equilibrium

To assess the state of the model from the initial condition at 200 Ma, we follow the evolution of average CMB heat flux and minimum dynamic topography. These two quantities are expected to be initially furthest away from equilibrium because the temperature field is synthetic with imposed subduction zones that correspond to dynamic topography lows.

2.1. Average core-mantle boundary heat flux

Fig. 3 shows that CMB heat flux is initially not in equilibrium for all cases. A thermal boundary layer was not included in the initial condition for cold cases, for which CMB heat flux initially increases sharply between 200-190 Ma. CMB heat flux then steadily decreases, and increases again as cold material reaches the CMB. This arrival occurs sooner in less viscous cases (see coloured tick marks on Fig. 3), and it precedes the minimum value of CMB heat flux by $\sim$ 10-25 Myr. This minimum is reached later in the model run ($\sim$ 100 Ma) for the more viscous cases, and earlier (between $\sim$ 165-150 Ma) for the less viscous cases. Hot cases reach a minimum CMB heat flux by 150 Ma, following an initial decrease. For case HH2, the CMB heat flux does not increase again, which could indicate that the amount of cold material initially inserted in the lower mantle for this case is closer to dynamic equilibrium for the assumed Rayleigh number. For low-viscosity cases, the CMB heat flux appears to oscillate around equilibrium from the first minimum, with a period $\gtrsim$ 160 Myr. However, high-viscosity cases show little CMB heat flux variation in the last 50 Myr. Taking the dynamic

thermal equilibrium as the half-amplitude of the oscillations, and assuming these would carry on beyond present-day for all cases, hot (cold) cases have been within $\sim$ 8% ($\sim$ 15%) of equilibrium since CMB heat flux reached a minimum.

2.2. Minimum dynamic topography

Fig. 4 shows that all cold cases and case HH1 are initially not in equilibrium for minimum surface dynamic topography that generally decreases between 200-180 Ma, then increases between 180-140 Ma and then plateaus, indicating that equilibrium has been reached, to the exception of case TC5 (temperature-independent viscosity) that does not reach equilibrium until $\sim$ 70 Ma. Case HH2 (shallower slabs in the initial condition) and case HH3 (low-viscosity asthenosphere) are initially closer to equilibrium for minimum dynamic topography and show less pronounced re-adjustments towards equilibrium.

References

Arriagada, C., Roperch, P., Mpodozis, C., Cobbold, P., 2008. Paleogene building of the Bolivian Orocline: Tectonic restoration of the central Andes in 2-D map view. Tectonics 27 (6), doi:10.1029/2008TC002269.

Bouysse, P., Palfreyman, D., 2000. Geological Map of the World at 1:25 M. Commission for the Geological Map of the World.

Boyden, J. A., Müller, R. D., Gurnis, M., Torsvik, T., Clark, J. A., Turner, M., Ivey-Law, H., Watson, R. J., Cannon, J., 2011. Next-generation plate-

tectonic reconstructions using GPlates. Geoinformatics: Cyberinfrastructure for the Solid Earth Sciences, 95–114.

Divins, D., 2003. Total Sediment Thickness of the World's Oceans and Marginal Seas. NOAA National Geophysical Data Center, Boulder, CO.

Gurnis, M., Turner, M., Zahirovic, S., DiCaprio, L., Spasojevic, S., Müller, R. D., Boyden, J., Seton, M., Manea, V. C., Bower, D. J., 2012. Plate tectonic reconstructions with continuously closing plates. Comput. Geosci. 38 (1), 35–42, doi:10.1016/j.cageo.2011.04.014.

Heine, C., Zoethout, J., Müller, R. D., 2013. Kinematics of the South Atlantic rift. Solid Earth 4 (2), 215–253, doi:10.5194/se-4-215-2013.

Montelli, R., Nolet, G., Dahlen, F., Masters, G., 2006. A catalogue of deep mantle plumes: new results from finite-frequency tomography. Geochem. Geophy. Geosy. 7 (11), Q11007, doi:10.1029/2006GC001248.

Ritsema, J., van Heijst, H. J., Woodhouse, J. H., 1999. Complex shear wave velocity structure imaged beneath Africa and Iceland. Science 286 (5446), 1925–1928, doi:10.1126/science.286.5446.1925.

Sandwell, D. T., Smith, W. H., 2009. Global marine gravity from retracked Geosat and ERS-1 altimetry: Ridge segmentation versus spreading rate. J. Geophys. Res.-Sol. Ea. 114 (B1), doi:10.1029/2008JB006008.

Simmons, N. A., Forte, A. M., Boschi, L., Grand, S. P., 2010. GyPSuM: A joint tomographic model of mantle density and seismic wave speeds. J. Geophys. Res.-Sol. Ea. 115 (B12), doi:10.1029/2010JB007631.

Srivastava, S., Verhoef, J., 1992. Evolution of Mesozoic sedimentary basins around the North Central Atlantic: a preliminary plate kinematic solution. Geol. Soc., London, S.P. 62 (1), 397–420.

Torsvik, T. H., Rousse, S., Labails, C., Smethurst, M. A., 2009. A new scheme for the opening of the South Atlantic Ocean and the dissection of an Aptian salt basin. Geophys. J. Int. 177 (3), 1315–1333, doi:10.1111/j.1365-246X.2009.04137.x.

Winterbourne, J., Crosby, A., White, N., 2009. Depth, age and dynamic topography of oceanic lithosphere beneath heavily sedimented Atlantic margins. Earth Planet. Sc. Lett. 287 (1), 137–151, doi:10.1016/j.epsl.2009.08.019.

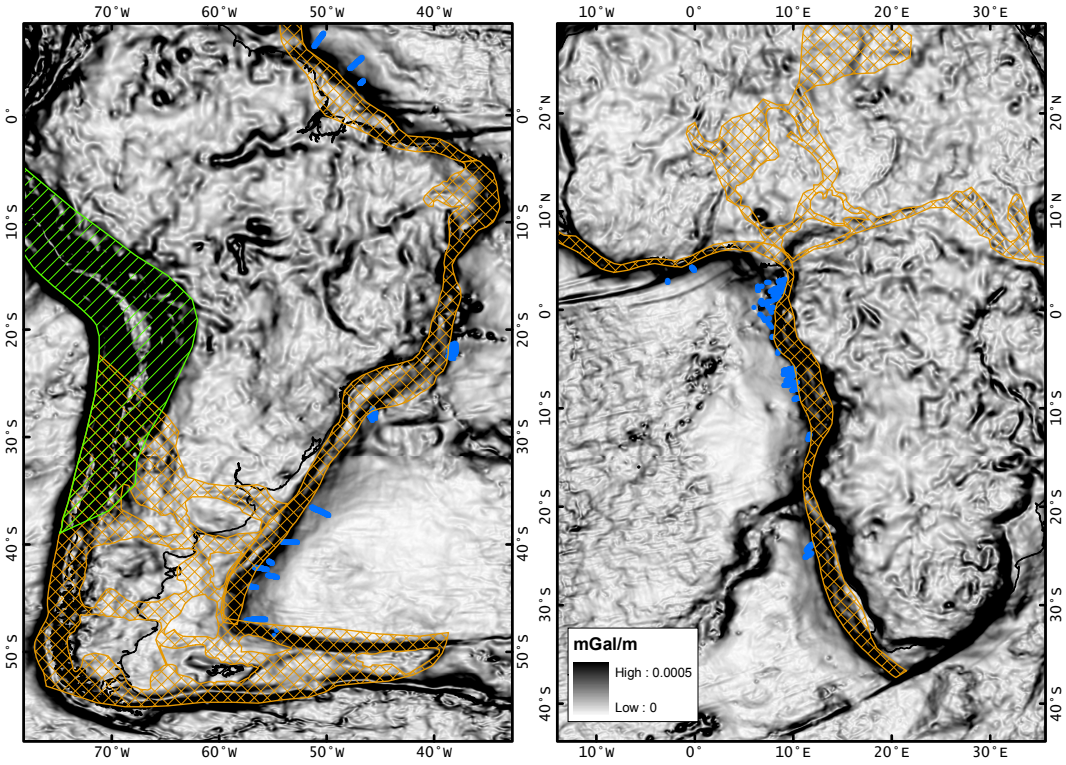

Figure 1: Total horizontal gradient of the 20 km upward continued Bouguer gravity. The landward limit of extended crust is defined to lie along the landward edge of large horizontal gradients. Regions within the orange hatched areas (here shown for the kinematic model of Heine et al., 2013) underwent deformation during Cretaceous South Atlantic opening. Green hatched region shows the extent of Cenozoic shortening in the Andes (adapted from Arriagada et al., 2008). Blue dots show extent of *bona fide* oceanic crust interpreted from seismic profiles by Winterbourne et al. (2009).

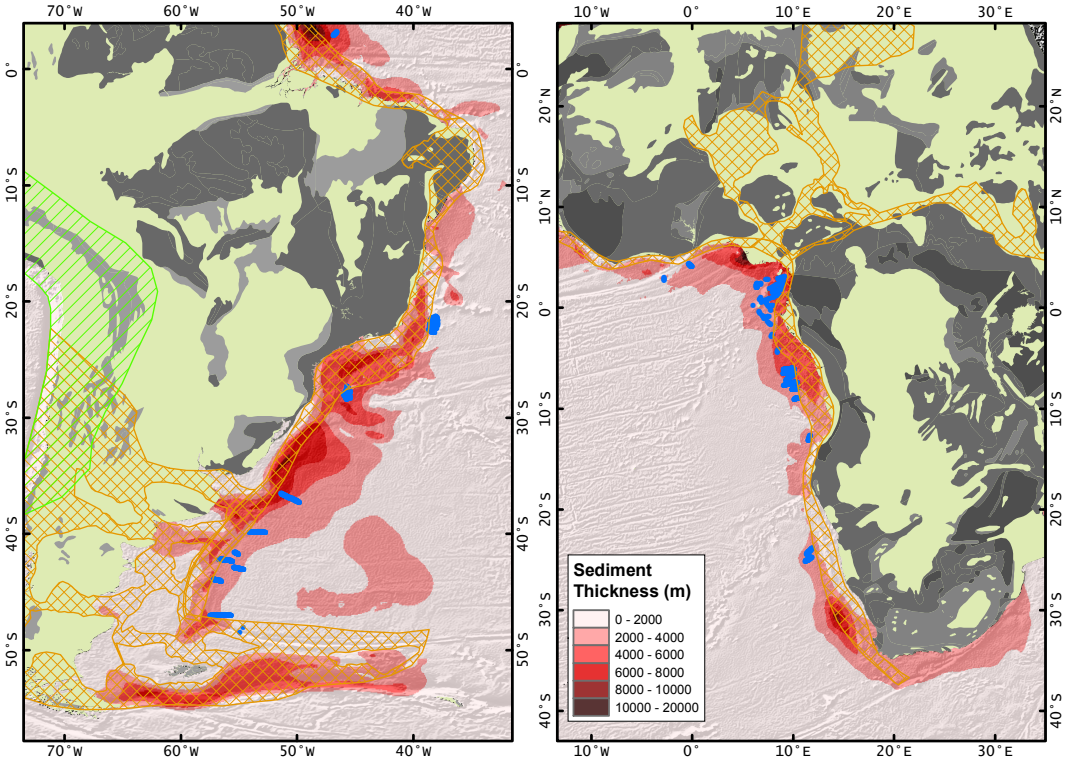

Figure 2: Offshore, the sediment thickness (Divins, 2003) is shown as shades of red, and the texture is derived from the gradient of free-air gravity anomalies based on satellite altimetry (Sandwell and Smith, 2009). Onshore, the surface geology (simplified from Bouysse and Palfreyman, 2000) is shown as shades of grey, with the light grey representing Paleozoic units and darker greys representing Proterozoic and Archean units. Deforming areas and *bona fide* oceanic crust are shown as in Supplementary Fig. 1.

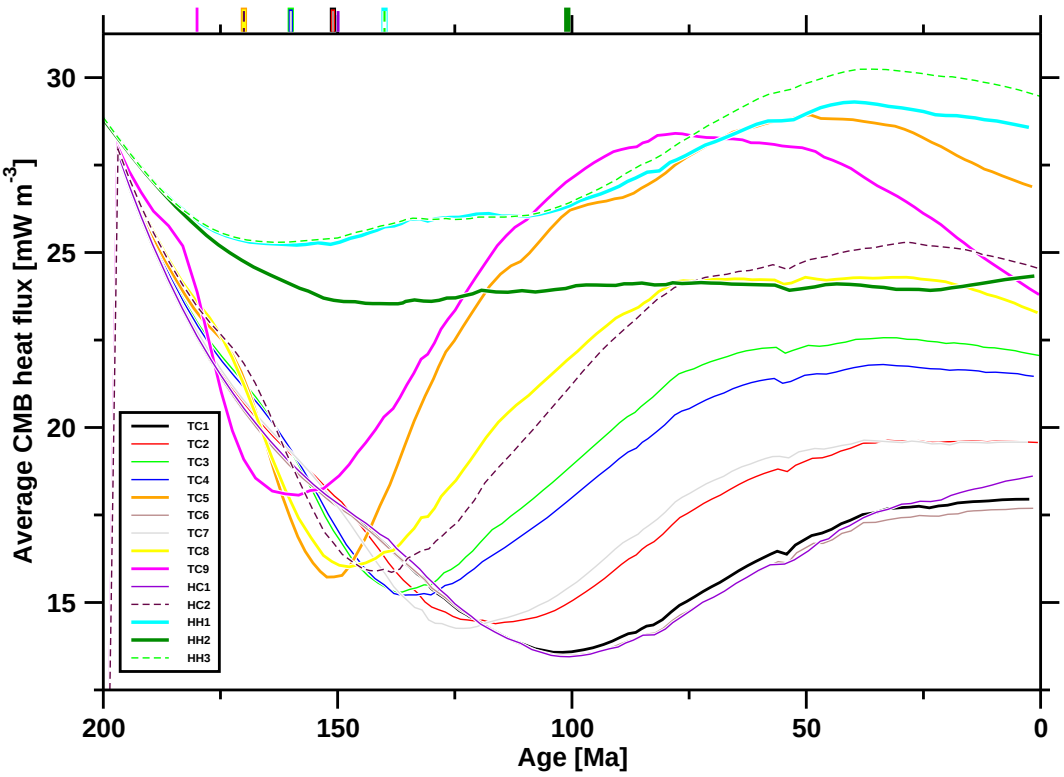

Figure 3: Evolution of average core-mantle-boundary heat flux for all cases. The tick marks at the top, coloured by model, indicate the first occurrence of cold material at $\sim$ 2810 km depth, detected visually.

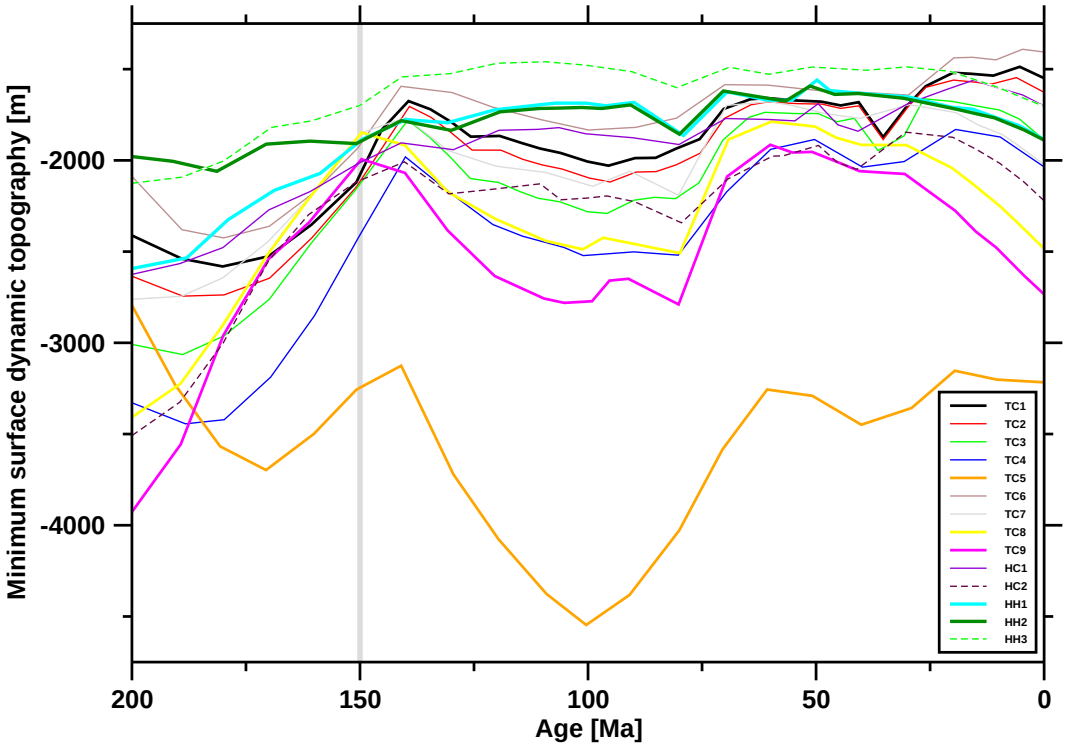

Figure 4: Evolution of minimum dynamic topography for all cases. The grey vertical line at 150 Ma indicates the age from which dynamic topography results are presented.

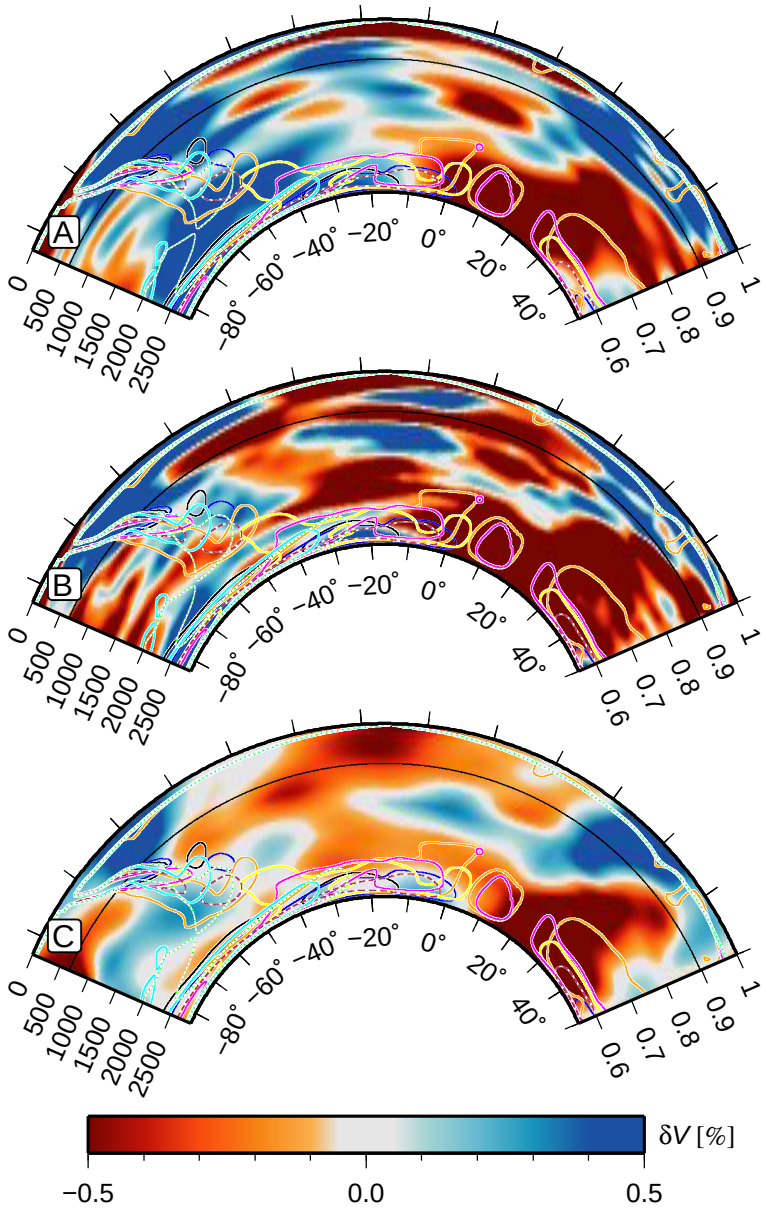

Figure 5: As Fig. 4B of the main text, for tomography A. S-wave model S20RTS (Ritsema et al., 1999), B. S-wave model GyPSuM (Simmons et al., 2010) and C. P-wave model of Montelli et al. (2006).

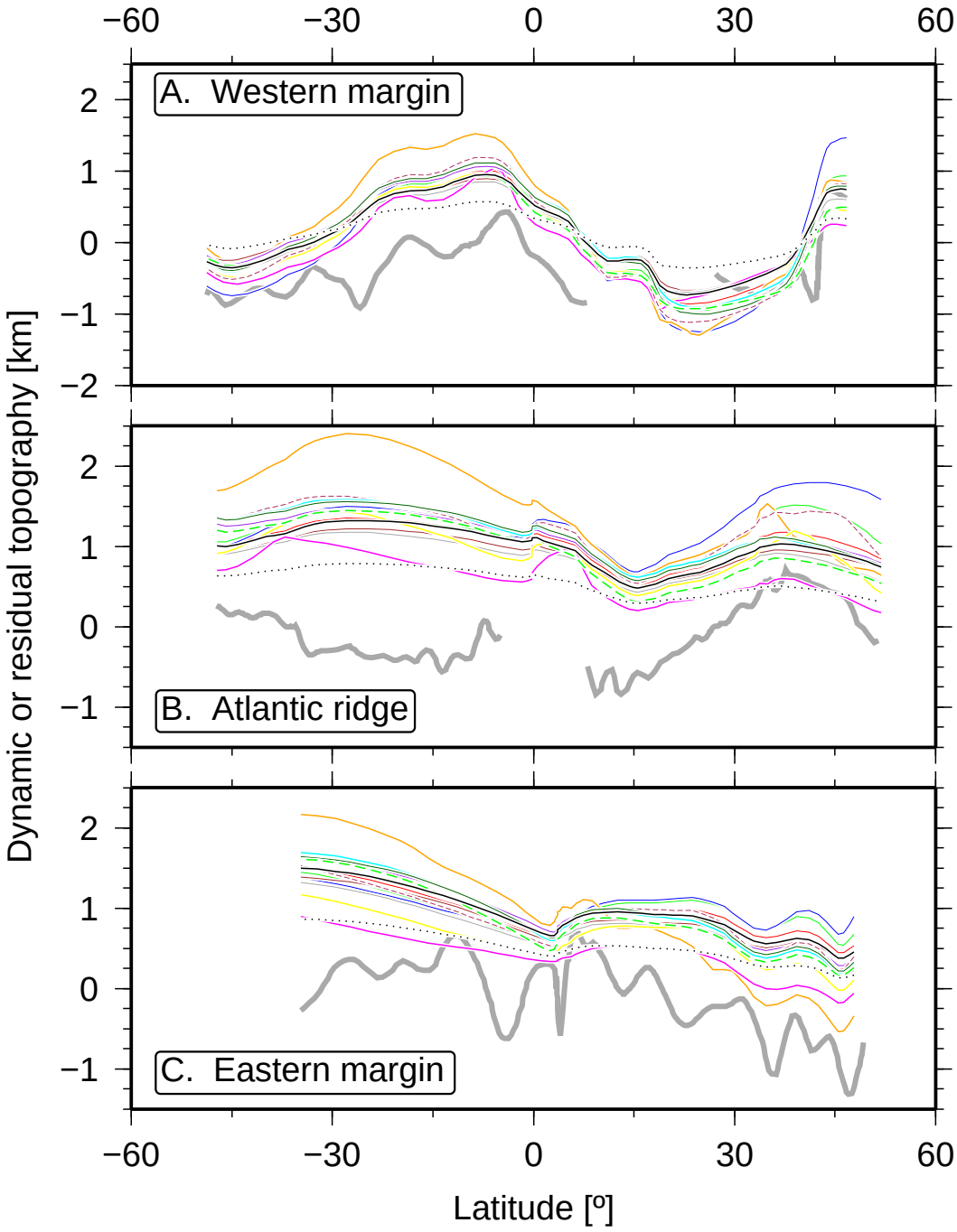

Figure 6: As Fig. 7A-C of the main text, for all modelled cases.

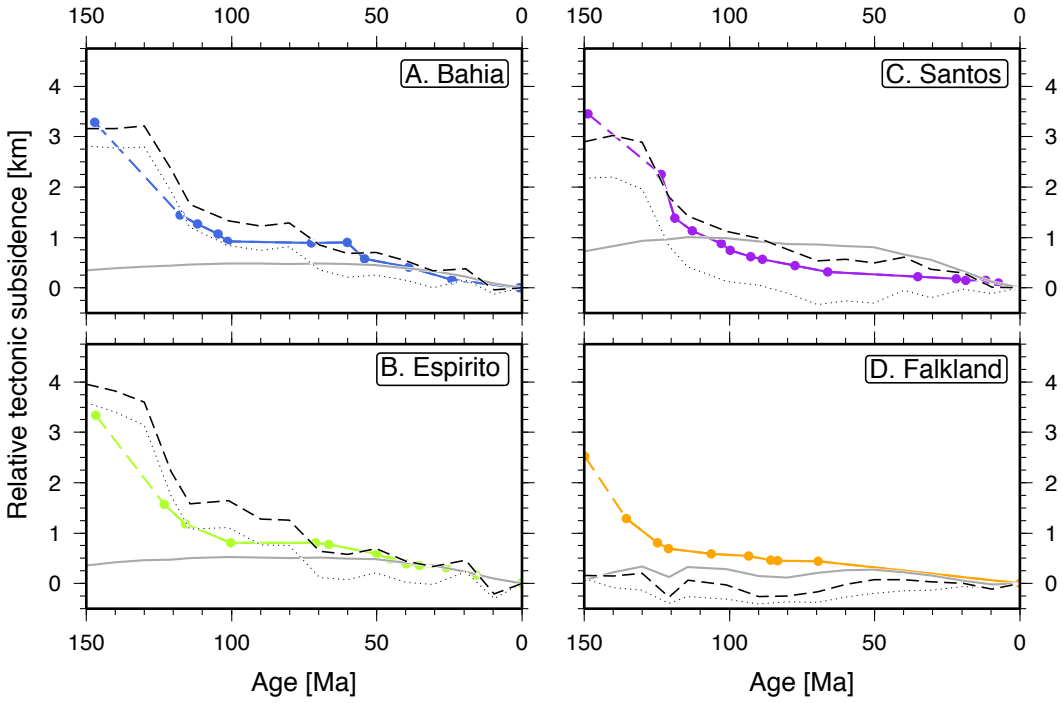

Figure 7: As Fig. 8A-D of the main text, for case TC4. The North Falkland basin is south of the deforming zone based on the reconstruction of Torsvik et al. (2009), therefore stretching is not predicted at that location.